Journal of Manufacturing Processes 120 (2024) 966–974

Contents lists available at ScienceDirect

Journal of Manufacturing Processes

journal homepage: www.elsevier.com/locate/manpro

Inkjet printing of a polymeric vibration damper for MEMS application adopting a step-reticulation process

Prisca Viviani [a], Maria Teresa Caporaso [a], Martina Scolari [b], Ilaria Gelmi [b], Laura Castoldi [b], Luca Magagnin [a,*]

[a] Dipartimento di Chimica, Materiali e Ingegneria Chimica "Giulio Natta", Politecnico di Milano, Via Luigi Mancinelli 7, 20131 Milan, Italy
[b] STMicroelectronics, Agrate Brianza 20864, Monza and Brianza, Italy

A B S T R A C T

In the frame of additive manufacturing techniques, inkjet printing (IJP) has gained great attention both from the academic and industrial point of view, for its customization, cost-effectiveness and simplicity, in contrast to more traditional patterning techniques, i.e. lithography. IJP could be flanked in the industrial manufacturing of parts of MEMS. In particular, since MEMS are constituted of mechanical parts, they are subjected to undesired vibrations that can degrade the device. In particular, polymers are optimal material candidates for vibration damping applications. The idea of the work was to demonstrate the possibility to adopt IJP for the production of a polymeric vibration damping layer on a floating spring of a MEMS device. In depth characterization of the polymeric ink is provided as well as a jetting characterization that helped the optimization of the printing process. A common reported issue of IJP is the impossibility to reproduce perfectly vertical walls, due to drops spreading when impacting the substrate. We tried to tackle this issue by proposing an alternative process, improving the verticality of the printed pattern walls. Printing was transferred to patterned MEMS and device characterization is proposed, in terms of how the printed polymeric layer can alter or not the mechanical properties of the spring. The work highlights how IJP can be adopted to produce components of devices, avoiding the use of expensive techniques.

1. Introduction

Over years additive manufacturing has gained growing interest and attention in applications where customization and cost-effectiveness are strategic features. In this frame, Inkjet printing (IJP) has emerged as a potential manufacturing process that can substitute more traditional patterning techniques, as lithography, where less exigent restraints on resolutions are required [1]. However, resolution in the micrometric range can be achieved, which is mainly limited, on the particle diameter, making this technique attractive for microfabrication [2]. Indeed, many devices feature microfabricated parts, as Micro-electro-mechanical systems (MEMS) [3]. Compared to more traditional surface patterning techniques, IJP is a contact-less, mask-less droplet-based technique able to deposit functional materials onto specific substrates following a digital pattern [4]. The possibility to finely control the thickness, by tuning the number of printed layers, combined with minimum material waste reveals the great versatility of this fabrication technique. For this reason, IJP has found applications in many fields, i.e. medicine [5], electronics [6,7], energy storage [8–10], biology [11], etc. Two main IJP operation modes exist: Continuous inkjet printing (CIJ) and Drop-on-Demand (DOD) inkjet printing [12]. While in CIJ drops are continuously ejected and then selected, in DOD system drops are ejected only when required and it is possible to achieve smaller features, with the possibility of reaching higher resolutions. However, major challenges of IJP are found on different levels. One is the long-term cartridges durability, as nozzle clogging is prone to occur. On the other hand, IJP requires precise ink rheological properties to guarantee flow under the application of a shear stress: low viscosity (i.e. 2–20 cP) and surface tension (i.e. 25–50 mN m^{-1}) [13,14]. Another important issue is the difficulty in achieving perfectly vertical walls, because of edges broadening. This aspect is mainly related to the spreading of drops that impact the substrate, because the solvent evaporation is not instantaneous and the printed material is subjected to flow. Unlike lithography, IJP features are always affected by this aspect, which represents one of the most important issue to address in microfabrication. In particular, IJP is also considered to be a key technology regarding polymers deposition and patterning tool [15–22]. Specifically, for UV-curable polymers printing, a possible approach to solve this issue is to adopt a step-reticulation process, which involves the UV reticulation of every printed layer, before printing the next one. Bernasconi et al. [23] have demonstrated the possibility to improve walls verticality and pattern uniformity adopting a step-reticulation approach. This approach can promote the use of polymers as candidate materials for vibration damping applications. Vibrations often represent a problem due to undesired motions

* Corresponding author.
E-mail address: luca.magagnin@polimi.it (L. Magagnin).

https://doi.org/10.1016/j.jmapro.2024.04.079
Received 30 November 2023; Received in revised form 19 March 2024; Accepted 23 April 2024

and stresses, that can lead to fatigue, failure, degradation and reliability loss for a wide range of structures in microelectronics. As MEMS devices consist of mechanical parts, they are prone to experience harsh undesired vibrations too, especially in case of accidental falls, that can lead to fracture of the mechanical component. There are two material classes for vibration control mechanism: active and passive damping [24]. The most common passive damping material are viscoelastic materials (VEMs), combining properties of elastic and viscous materials, where damping occurs by energy dissipation due to friction among oligomers chains under cyclic deformation. VEMs may be used as discrete dampers, absorbers covering the surface of the structure, e.g., fully or partially. As a matter of fact, a common viscoelastic treatment to control vibrations in a structure is the free-layer damping (FLD) approach. The damping material is deposited on the structure surface, creating a damping layer. When the structure is deflected, vibrations are damped because of the energy dissipated following the compression/extension of the damping material [25,26].

With this work, we demonstrated how IJP can be adopted as an alternative microfabrication technique for MEMS and functional parts manufacturing and how can be adopted to deposit material on floating substrates. A complete characterization of the polymeric inks, the adopted waveform, the jetting and their printing will be provided. Eventually, the polymeric material will be deposited on floating substrates, i.e. spring, present on patterned wafers and characterized accordingly in terms of profilometry and spring deflection.

2. Experimental & characterization

2.1. Ink preparation & characterization

The adopted polymer was a solvent-free UV-curable acrylate (Delo®Photobond® 4436 from Delo). Cyclopentanone (CP) was purchased from Sigma and was used as solvent to dilute the acrylate in order to make it compatible for IJP. Different mass concentrations of acrylate polymer were adopted and characterized, i.e. 33 % (1:2 wt%), 25 % (1:3 wt%), 16 % (1:5 wt%) and 9 % (1:10 wt%). Once the acrylate was added to CP, the mixture was stirred for 5 min. During this time, the solutions were covered with an aluminum foil to avoid any premature reticulation. The printed material was cured by exposition to a 400 nm UV lamp for 10 min, during which samples were also expose to N_2 flow to create an inert atmosphere, which was needed to ensure a complete reticulation. Additionally, the step-curing approach was performed by exposing each printed layer to a 400 nm UV lamp for 10 min, under N_2 atmosphere, before printing the next one. Inks were characterized in terms of viscosity and surface tension. Viscosity was measured a Rheometrics DSR200 (Dynamic Stress Rheometer) with planar plates (20 mm) and a fixed height of 0.4 mm. Flow curves were acquired by increasing the shear rate up to 10 k s^{-1}. Surface tension measurement was performed by pendant drop technique and drop shape analysis fitted through Opendrop software. Contact angle was performed by ejecting a precise amount of material on SiO_x substrate and applying an optical analysis of the drop.

2.2. Inkjet printing

The inks were printed using a Ceradrop F4-Series (MGI group). The printed had various modules, one supporting disposable cartridges (Fujifilm Dimatix). Inks were transferred in 10 pL disposable cartridges, with a nozzle diameter of 21 μm. Following the optimization of the rheological properties of the ink as well as of the jetting and printing conditions, a waveform and jetting characterization were performed, in order to find the best printing conditions in terms of particle velocity, trajectory and absence of satellites particles. Regarding printing parameters: a jetting frequency of 1 kHz was adopted, printing height was fixed to 1 mm from the substrate, the platen was either kept at room temperature or heated up to 60 °C, the maximum value allowed.

2.3. Printing characterization

A preliminary pattern consisting of an array of squares 0.8 mm × 0.8 mm was printed on a SiO_x wafer. Once found the best printing conditions, a pattern provided by StMicroelectronics was printed with a target thickness of 15 μm, which was then transferred to the wafer where all the devices were present. Alignment of the head with the substrate was performed through DriverCeraprinter software. Once reticulated, all printed patterns were characterized in terms of profilometry, in order to verify the obtained thickness. A KLA Tencor profilometer with a stick of 5 μm radius tip was used, using a scanning speed of 20 μm/s with a sampling rate of 20 Hz and an applied force of 1 mg.

2.4. Device characterization

The spring deflection measure was performed with a metrological tool (NSX330, ONTO) that reconstructed the superficial profile of the sample through a technique exploiting a confocal laser. The measure involved acquisition of the profile along the line reported in Fig. S7, taking the heights of three points:

- Points A and B: are used to normalize the profile and define a “zero” height;
- Point C: at the center of the mobile structure of the device where the height was defined.

Height of the point C was very susceptible in terms of stress, that caused torsion of the spring. To the measured height, the thickness of the printed layer was subtracted.

3. Results & discussion

3.1. Ink characterization

The starting material was a one-component solvent-free acrylate, which was not compatible with IJP in its undiluted form, since its viscosity, i.e. 350 mPa s, was not in a desirable range for IJP, i.e. 2–12 mPa s. Cyclopentanone (CP) was used to dilute the acrylate, since a good dispersion and miscibility were obtained. Table S1 collects physical properties of the acrylate and CP. In particular, CP was chosen because of its low viscosity and medium-high boiling point. This latter aspect favored a sufficiently fast evaporation of the solvent after printing and prevented nozzle clogging due to too fast solvent drying. Four dilutions were prepared by varying the solute-solvent weight ratio, i.e. 1:2, 1:3, 1:5 and 1:10, respectively. For each dilution, relevant physical properties as viscosity, surface tension and density were measured in order to calculate the Ohnesorge (Oh) (1) and Reynold (Re) (2) numbers:

$$Oh = \frac{\eta}{\sqrt{\sigma \rho d}} \tag{1}$$

$$Re = \frac{\rho d v}{\eta} \tag{2}$$

where η is the dynamic viscosity of the ink, σ is the surface tension, ρ is the density of the ink, d is a characteristic length, typically the nozzle diameter, and v is the drop velocity. Table 1 reports the measured physical properties for four dilutions. Values variation according to

Table 1
Surface tension, density and viscosity values of different solutions with different dilutions, i.e. 1:2, 1:3, 1:5 and 1:10 (wt%).

	1:2	1:3	1:5	1:10
Surface tension (mN m^{-1})	26.95	27.89	29.47	33
Density (kg m^{-3})	966	962	958	955
Viscosity (mPa s)	8.07	5.38	3.52	2.22

different solvent quantity was in accordance with what expected. In particular, flow curves were acquired in order to evaluate viscosity values at high shear rates. Fig. 1a shows flow curves of the four dilutions, where viscosity values decreased by increasing the polymer dilution. It was important to evaluate viscosity values in the high shear rates region, as they were in fact representative of the ink viscosity values during the ejection phase, where high shear rates are typically involved, i.e. 10^4–10^5 s^{-1}. All the four dilutions showed a Newtonian-like behavior, meaning that the viscosity was independent from shear rates. This was particularly helpful, as viscosity values were still in the accepted range for IJP at high shear rates. The typical Oh/Re printability diagram was then built, through which it was possible to provide a theoretical justification of the printability (or not) of the inks. Fig. 1b shows the Oh-Re diagram for four dilutions. In order to calculate Oh/Re values, nozzle diameter was fixed to 21 μm and using different drop velocity, i.e. 2 m s^{-1}, 5 m s^{-1}, 10 m s^{-1} and 15 m s^{-1}. Dilution 1:10 was the only one found out of the range of printability (green area), as Oh < 0.1, implying the possible formation of satellites. However, this condition has been revisited: lower Oh values are still acceptable, as satellites can be reabsorbed in the main drop before impacting the substrate [16]. For each dilution, the lowest and highest velocity gave undesired conditions, as the droplets couldn't be ejected because of insufficient kinetic energy or produced onset of splashing, respectively, meaning that their speed were either too low or high. Specifically, we adopted the 1:3 dilution, as it was the most concentrated solution that we were able to print, without causing nozzle clogging.

3.2. Jetting characterization

Jetting characterization was performed in terms of waveform optimization, in order to find the best printing conditions that could give the ejection of satellites-free, spherical and sufficiently fast drops. All these requirements were necessary to ensure the best quality of the final print. Fig. 2a represents the adopted mono-pulse waveform. It was possible to control the voltage level, the slew rate and duration of the pulse. We decided to focus on the effect of the variation of both the slew rate and voltage level. To compare the effect of different slew rates, we kept constant the voltage level fixed at 20 V and the pulse duration. Fig. 2b-d represents photograms of the droplets taken at different times after the ejection, upon variation of the slew rate of the waveform. A too steep slew rate (blue waveform) produced drops with too high velocity, i.e. > 5 m s^{-1}, with satellites defects (Fig. 2b). A too low slew rate (red waveform), on the contrary, produced too slow drops, i.e. < 5 m s^{-1} (Fig. 2d). A condition in between the previous two was the optimal one which provided spherical, satellites-free drops with an optimal velocity around 5 m s^{-1} (Fig. 2c). All these observations were in accordance with the fact the slew rate of a waveform is associated to how fast the piezoelectric element is deformed, thus associated to the drop speed after ejection [27]. The other studied parameter was the voltage level. In particular, drop velocity was studied according to the voltage variation and the temperature applied to the nozzles. Fig. S1 represents the drop velocity change upon different voltages and temperatures applied to the nozzles. In agreement with literature [28,29], it was found a linear correlation of drop velocity with voltage increase. The minimum voltage that allowed the ejection of a drop was 18 V at room temperature to which a drop velocity of 2 m s^{-1} corresponded. The highest allowed voltage of 40 V produced a drop whose speed was 8.5 m s^{-1}. However, these limit conditions did not favour an optimal jetting because of unsuitable drop speeds and presence of satellites. In addition, drop velocity increased by increasing the applied heat to the nozzles, fixing a voltage. This found a justification considering a decrease of the ink viscosity upon an increase of temperature, thus the ink resulted to be easier to be jetted. A voltage of 27 V with the nozzle kept at room temperature was found to be the optimal one, allowing the ejection of a spherical, satellite-free drop with a speed of 5 m s^{-1}.

3.3. Substrate interaction

Evaluation of the polymer-solvent system interaction with the substrate, i.e. SiO_x, was considered in order to achieve a good quality of the final print. In this context, substrate wettability was a parameter of interest, which is linked to the drop surface tension to determine the droplet contact angle with the substrate. The measured contact angle of the ink on SiO_x was around 18° (Fig. S2): the drop was in fact well spread on the substrate, meaning that there was good wettability. In particular, droplet contact angle combined with droplet diameter before and after the impact with the substrates were used to determine the maximum drop spacing (Δx_{max}) (3):

$$\Delta x_{max} = \frac{2\pi D_0}{3\frac{D^2}{D_0^2}\left(\frac{\theta_{eq}}{sin^2\theta_{eq}} - \frac{cos\theta_{eq}}{sin\theta_{eq}}\right)} \quad (3)$$

where D_0 is the droplet diameter before the impact, D is the droplet diameter after the impact and θ_{eq} is the contact angle. Drop spacing describes the degree of overlapping of adjacent drops. If the drop spacing is greater than the distance between the centers of two adjacent drops, no drops coalescence will be obtained. This leads to a non-continuous pattern, with voids due to incomplete coalescence of

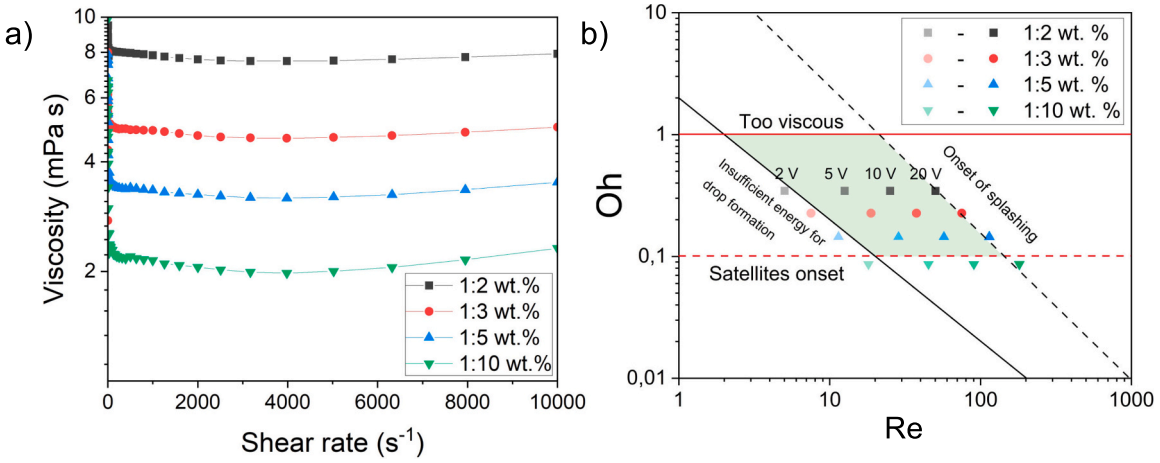

Fig. 1. Flow curves of differently diluted inks (a) and Ohnesorge-Reynold printability diagram of differently diluted inks upon voltage (thus, drop speed) variation (b):s black square 1:2 wt%, red circle 1:3 wt%, blue triangle 1:5 wt% and green reversed triangle 1:10 wt%. (For interpretation of the references to colour in this figure legend, the reader is referred to the web version of this article.)

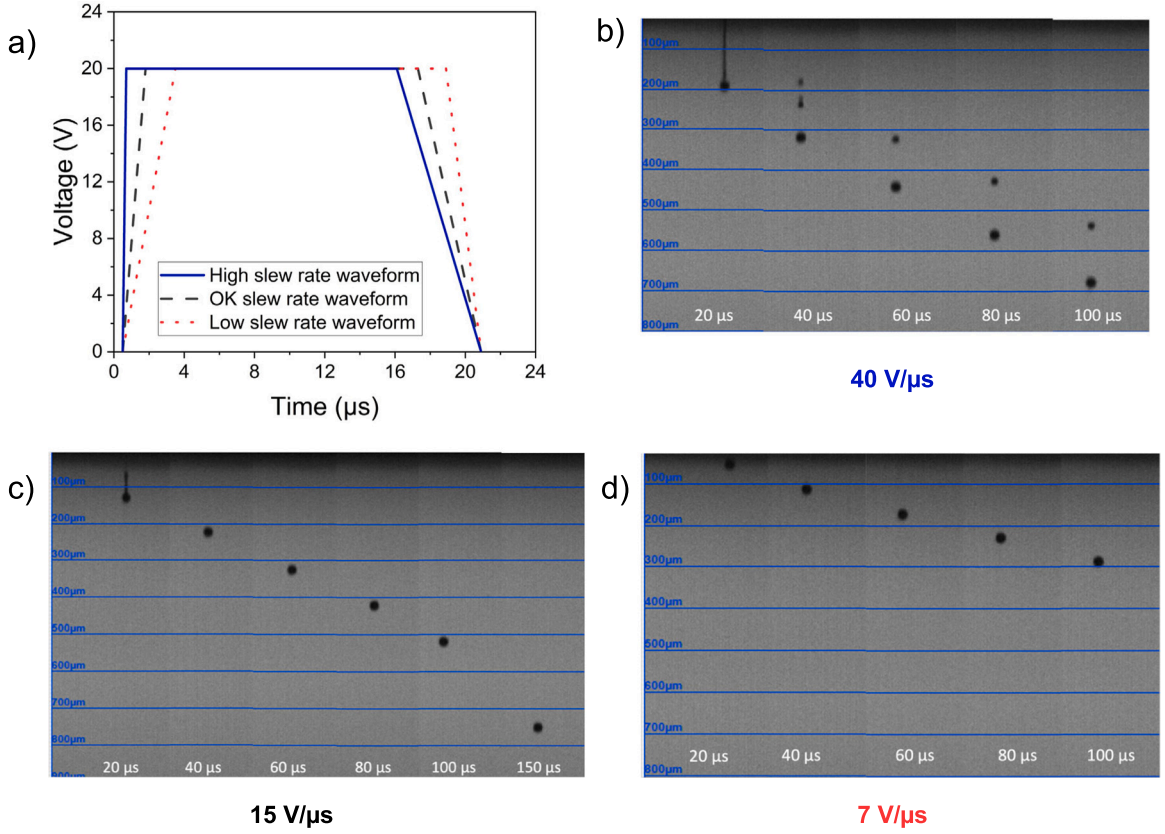

Fig. 2. Different waveforms where slew rate was varied: high slew rate (blue), ok slew rate (black) and low slew rate (red) waveforms (a) and photograms taken at different times after ejection representing the evolution of the ejected drops associated to high slew rate waveform (b), ok slew rate waveform (c) and low slew rate waveform (d). (For interpretation of the references to colour in this figure legend, the reader is referred to the web version of this article.)

drops. Δx_{max} was calculated considering the measured θ_{eq}, D_0 that was provided by the DriverCeraprinter software that was around 29 μm and D that was measured printing an array of separated drops on SiO_x either kept at room temperature and at 60 °C. Fig. S3 reports different profilometries of two drops printed on SiO_x substrate kept at room temperature and 60 °C. The difference in terms of thickness, profile and diameter was evident: the thickness of the drop printed at room temperature was around 0.4 μm with a spread profile and a D = 61 μm, while the drop printed at 60 °C showed sharper edges, with a consequent higher thickness of about 0.9 μm and a D = 33 μm. These differences were ascribable to a faster solvent evaporation when a drop impacted a heated substrate. The calculated Δx_{max} was around 65 μm in the case of substrate kept at room temperature. This value will be confirmed experimentally in the next section. Concerning the Δx_{max} calculation in the case of the substrate kept at 60 °C, Δx_{max} was empirically found as it was not possible to measure θ_{eq} at 60 °C.

3.4. *Printing characterization – squares array*

An array of squares (800 μm × 800 μm) was printed on SiO_x wafer kept at room temperature varying the degree of drop overlapping, i.e. drop spacing, from 20 μm to 70 μm, the latter being beyond the maximum drop spacing. Fig. 3b shows the thickness variation of one printed layer upon drop spacing variation. Effect in changing the drop spacing was evident: when increasing the drop spacing (but still below the Δx_{max}), i.e. increasing the distance between two adjacent overlapping printed drops, the thickness sensibly decreased. The contrary occurred when decreasing the drop spacing, as the overlapping degree among droplets was increased. Fig. 3a reports optical images of one printed layer single squares printed with different drop spacing. Effect in changing the drop spacing was also optically evident. An increase of the iridescent colored area, which is associated to a low-thickness area, was more obvious when decreasing drops overlapping. Scalloping effect was evident starting from Δx_{max} = 50 μm, as the drops were poorly overlapped. At Δx_{max} = 60 μm early signs of drops mis-coalescence were evident, while using a $\Delta x > \Delta x_{max}$ = 70 μm made impossible to obtain a continuous printed layer, as drops were printed too much far apart to coalesce, confirming the calculation of Section 3.3. Fig. 3c shows the profilometry of one printed layer squares, which gave an idea of how the material was redistributed along the section. Profilometries highlighted a typical IJP defect: the coffee ring effect (CRE), which is associated to the accumulation of material at the edges of the prints due to a faster solvent evaporation in this area [30–36]. CRE was more evident as the drop spacing increased. At this point, a higher number of layers was printed. Fig. 3d shows the thickness evolution by varying the number of printed layers and the drops spacing. In agreement with previous results, fixing a number of printed layers, a higher thickness was achieved decreasing the drop spacing. In particular, adopting Δx = 20 μm it was possible to reach a thickness of 9 μm with five printed layers. Since a minimum thickness of 15 μm was required for the MEMS damping layer, it was important to find the best conditions to reach the target thickness printing the minimum number of layers in order to not affect the final print resolution. Print resolution was in fact affected by three main aspects: accumulation of material at the edges, lacking walls verticality, which is another peculiar defect in IJP linked to drop spreading, and broadening of the pattern. Fig. 3e shows the degree of pattern broadening along the parallel and perpendicular printing direction for Δx = 20 μm. Pattern broadening increased by increasing the number of printing layers until a plateau value, as more material was progressively deposited. In particular, it was found that pattern broadening had a dependence on the printing direction: it was higher along the perpendicular direction of printing, compared to the parallel one. This may be

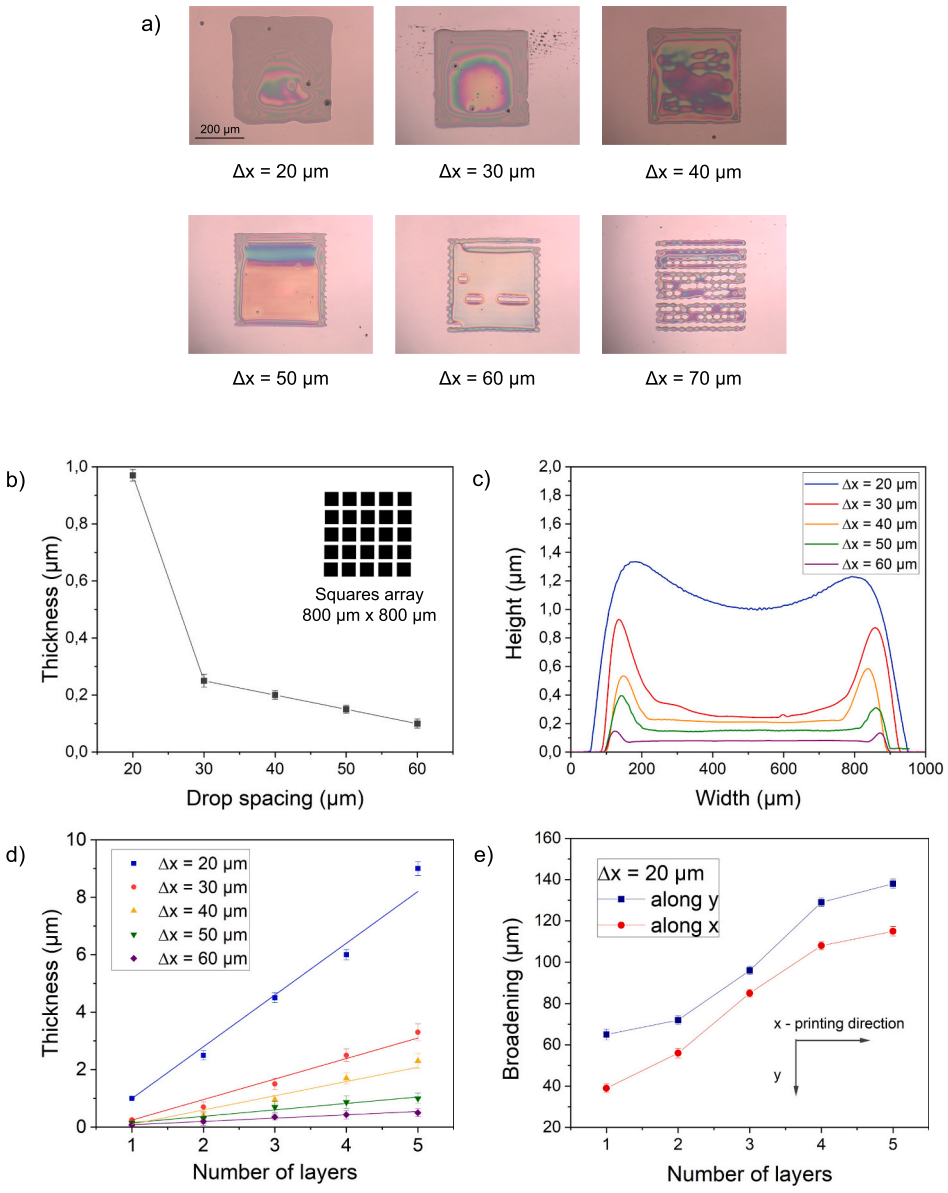

Fig. 3. Optical images of one printed layer single squares printed with different drop spacings (Δx = 20 µm – 70 µm) (a), thickness evolution by varying the drop spacing of a printed square, inset: 800 µm × 800 µm squares array (b), profilometry of printed squares corresponding to different drop spacing (c), thickness evolution upon different number of printed layers and drop spacing values (d) and pattern broadening variation varying the number of printed layers and drop spacing (e).

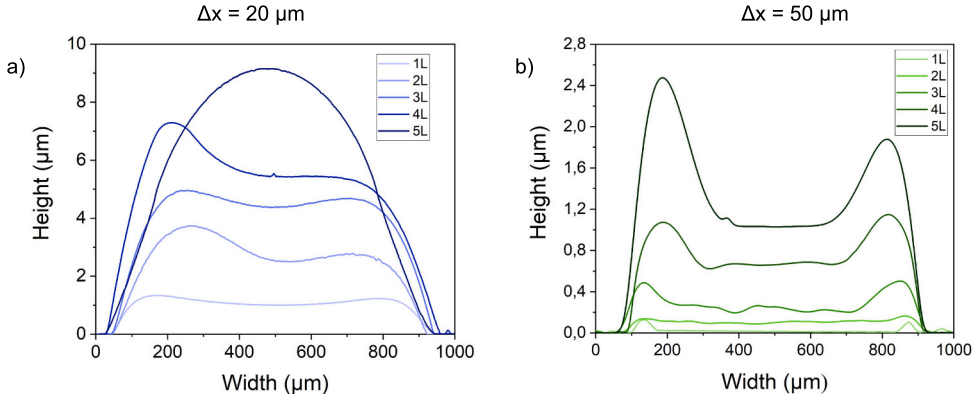

Fig. 4. Profilometries of one up to five printed layers of a square pattern using Δx = 20 µm (a) and Δx = 50 µm (b) on a SiO_x substrate kept at room temperature.

ascribed to the fact that drops immediately coalesce along the printing direction, contrary to what happens along the perpendicular direction. In addition, Fig. 4a-b shows the profilometries of one up to five printed layers of a square pattern using Δx = 20 μm and Δx = 50 μm, respectively, evidencing the CRE dependence on drop spacing.

At this point, the role of increasing temperature of the substrate, up to 60 °C, was evaluated, in order to compare the differences in terms of thickness and profilometries. In Section 3.3, the variation of drop shape and diameter when printed on 60 °C substrate was discussed. Fig. 5a reports optical images of one printed layer single squares printed with different drop spacing keeping the substrate at 60 °C. Also in this case, the effect of drop spacing variation was evident, as an increasing iridescent area was evident by decreasing the drops overlapping. Specifically, we found that Δx > 50 μm produced incomplete, non-homogeneous patterns, with scalloping effect, due to a too large distance between printed drops. The decrease in Δx_{max} was ascribable to a higher chuck temperature that induced less broadening, because of a faster solvent evaporation. We decided to test only Δx = 20 μm Δx = 30 μm, since only with these values it was possible to reach sufficiently high thicknesses, in an optic where minimizing the number of printing layers was beneficial for the final resolution. Fig. 5b shows the thickness comparison between prints on SiO_x substrate at room temperature and 60 °C upon variation of the number of printed layers and of the allowed drop spacings, i.e. 20 μm and 30 μm. For both drop spacings, results have shown that a higher thickness was reached when printing on a heated substrate, again linked to less spreading of the ink when deposited on the substrate. In particular, it was possible to achieve a thickness of 11 μm by printing five layers using a drop spacing of 20 μm, about 2 μm thicker compared to the same print but using a substrate at room temperature.

Fig. 5c compares the pattern broadening of prints on heated and non-heated substrate upon variation of number of printed layers and drop spacing along the perpendicular direction. As expected, pattern broadening was lower when increasing from Δx = 20 μm to Δx = 30 μm, as less material was printed. In addition, pattern broadening sensibly decreased when printing on a heated substrate, which was ascribable to a faster solvent evaporation that partially inhibited or limited material spreading. Fig. 6a-b reports the profilometries of one up to five layers of a printed square pattern using Δx = 20 μm and Δx = 30 μm, respectively. The increase in chuck temperature favours a more homogenous material redistribution, thus smoothing and limiting uneven accumulation of material toward the edges. Given all the results, it was possible to select the printing conditions in order to achieve the best quality of final print. A drop spacing of 20 μm combined with printing on a heated substrate will be adopted from now on to print the final pattern and characterize it.

3.5. *Printing characterization – final pattern*

Fig. S4a reports the CAD file of the so-called “final” pattern, the one that will be printed on top of the spring present on the MEMS device. Critical features were present, whose dimension was around ~170 μm, which were not trivial to obtain. Adopting the previously optimized printing parameters, we printed the final pattern first on a SiO_x wafer characterized by different printing layers. Fig. 7a represents the optical images of printed final pattern with different number or printed layers, adopting a non-step and a step-reticulation process. Non-step reticulation process involved printing of all the desired layers and, only after, reticulating them. Looking at the evolving series of the prints from one

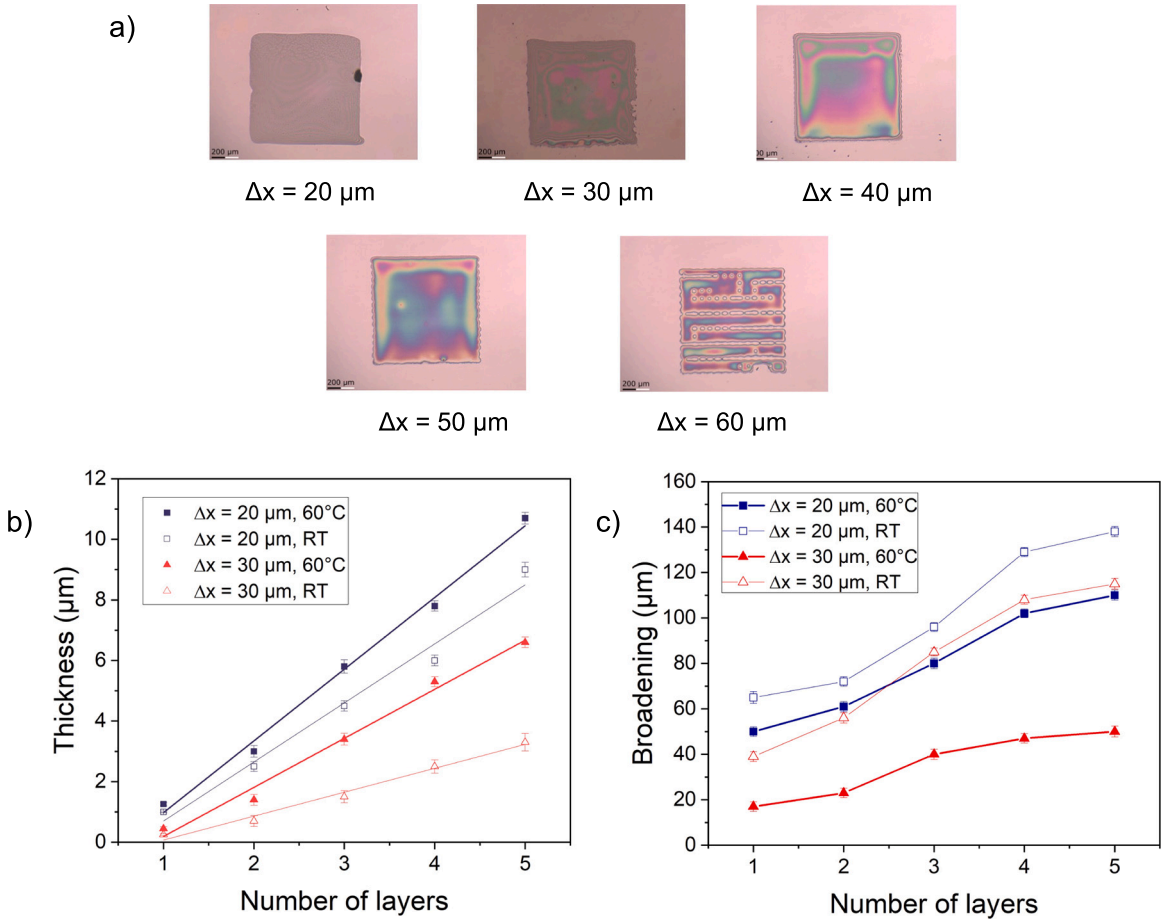

Fig. 5. Optical images of one printed layer single squares printed with different drop spacings (Δx = 20 μm – 60 μm) (a), comparison of thickness evolution (b) and pattern broadening (c) between prints on SiOx substrate kept at room temperature and heated to 60 °C upon variation of number of printed layers and drop spacing.

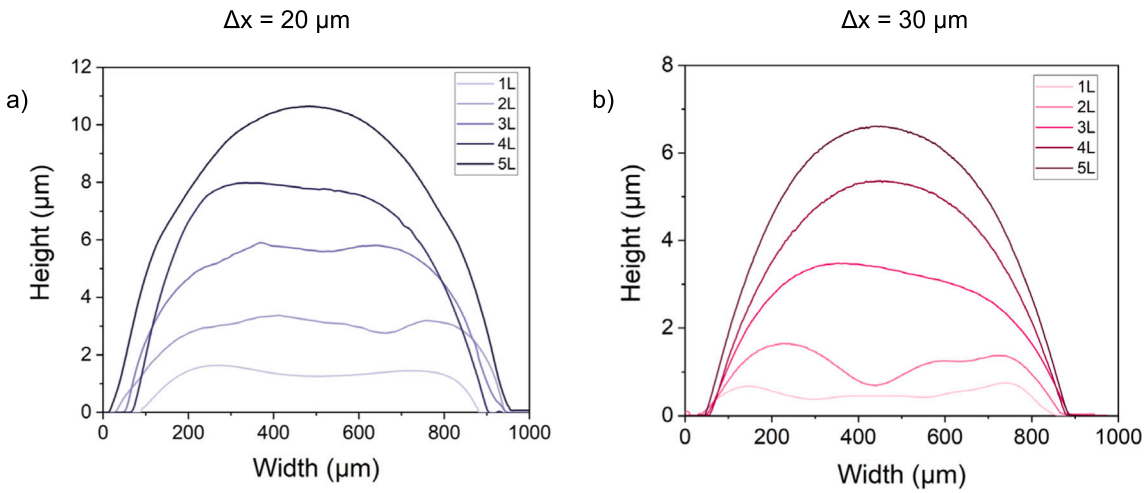

Fig. 6. Profilometries of one up to five layers of a printed square pattern using $\Delta x = 20$ μm (a) and $\Delta x = 30$ μm (b).

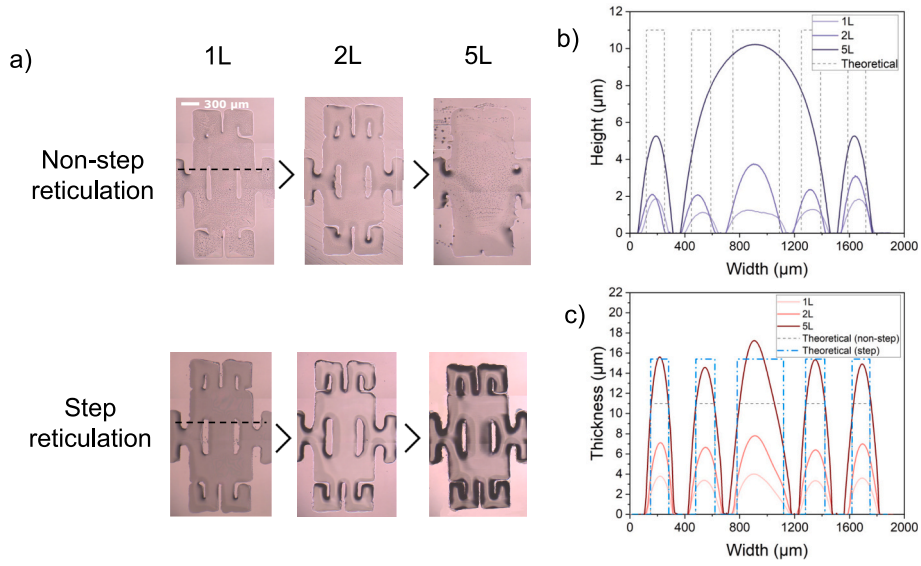

Fig. 7. Optical images of the printed final pattern with different number of printed layers and comparing the effect of using a non-step and a step reticulation process (a). Corresponding profilometries of different printed layers of the final pattern obtained with non-step (b) and step-reticulation process (c).

to five layers, this had the effect of generating a strong broadening of the printed material, as previously seen, which caused the loss of all the finest features present in the final pattern. This was also visible from the corresponding profilometry that was done in correspondence of the dashed line (Fig. 7b). In particular, the profilometries of one and two printed layers were quite in line with the expected pattern, with all the features still visible, and a good homogeneity in terms of thickness. However, five printed layers produced a completely spread profile, where all the features and resolution were lost, i.e. the theoretical profile was completely lost. These aspects produced inhomogeneities in terms of thickness, as well, with the printed material flowing from the outer region toward the more massive central one. A solution to this effect was found in adopting a step-reticulation process, where reticulation occurred at every printed layer, before printing the next one. In this way, the new material printed could not in fact merge with the one already printed, limiting any possible broadening effect. This effect was clearly visible from the optical images, where the five printed layers pattern still showed all the most critical features. This was also confirmed by the profilometry reported in Fig. 7c: the five layers profilometry followed the theoretical expected pattern (blue dashed dotted line) of a step-cured 5 L printed pattern. This latter differs from the theoretical one obtained with a non-step approach because of a higher thickness, i.e. ~ 15 μm, because of a lower solvent spread. In addition, the walls were still not perfectly vertical, but walls verticality was sensibly improved, following as much as possible the theoretical pattern. Interestingly, the obtained thickness (~ 15 μm) was higher compared to the expected one and it was somehow homogeneous along all the pattern. Fig. S4b shows the optical image of a total of five printed layers of the final pattern, obtained with a step-curing approach, i.e. curing the printed layer before printing the next one. Comparing the obtained printed pattern with the original design, it is evident how the step-curing approach sensibly improved the final resolution of printed product, i.e. the print faithfully reproduced the pattern. For instance, the printed central section, which in its original design measured ~920 μm, measured ~935 μm, giving a broadening of ~15 μm. In addition, critical features denominated as “A” and “B” showed a broadening of ~7 and 8 μm, respectively, when compared to the dimensions of the original design. Overall, adopting a step-reticulation process produced prints that demonstrated the possibility to IJP complex designed patterns with an accurate reproduction of details given by the design. At this point, it was possible to transfer the print on the springs present on the MEMS devices. At this stage, a careful alignment of the printhead and the patterned wafer was performed, in

order to create a good alignment of the print origin. In particular, it was important to consider the existence of a print offset, that originated from the printhead motion. Drops won't end up in a perpendicular position with respect to the nozzle from which it was ejected, but in a shifted position because of inertia. The difference between the real shifted position and the expected perpendicular one was the print offset. This effect is explained in Fig. S5a and reported in the corresponding images, where the printed pattern is misaligned on the x direction due to the existence of an offset. Taken this precaution, it was possible to obtain precisely aligned prints with the spring present on the devices. Fig. S5b shows the device before printing the damping layer, while Fig. S5c shows the same device after printing five layers of the polymeric ink adopting a step-reticulation process. It is worth to highlight how the step-curing approach could be adopted for the production of real functional parts on patterned wafers. Despite the presence of slight broadening outside the desired area, the overall print was successfully aligned with the spring. Ultimately, Fig. S6 shows an optical profilometry performed on the MEMS device with five printed polymeric layers, showing some issues related to inhomogeneities of the thickness along the pattern.

3.6. Device characterization

Device characterization was performed by evaluating the spring deflection upon variation of the number of printed layers of the polymeric material. The spring had specific mechanical properties and the addition of layers of polymeric material may change the stress of the structure, thus altering the device response. Fig. S7 shows the measure of the height deflection of the spring. Scattering of the measured points (red circle) was related to the transparency of the printed polymeric layer; the thickness of the printed polymeric layer was subtracted to the measured average value. Results related to the deflection of the spring according to the number of printed layers are reported in Table 2. The maximum acceptable deflection, after which an alteration of the spring mechanical properties would be achieved, was set to $-25\ \mu m \pm 5\ \mu m$. For five printed layers, the achieved height of the structure was -12.55 μm, which was in an acceptable range. Ultimately, spring response was proved to be unaffected by the polymeric layer.

4. Conclusions

The aim of this work was to demonstrate the possibility to adopt IJP as an alternative manufacturing technique that can be flanked to more traditional surface patterning techniques in applications where no challenging restraints on resolution are needed. The best printing process parameters were determined, in order to achieve a free-clogging jetting and smooth printing process. This was done through a deep understanding of the rheological and physical properties of the polymeric-based ink. A jetting characterization was proposed, in terms of waveform optimization, as well as an analysis of the ink interaction with the substrate. The effect of drop spacing was considered and $\Delta x = 20\ \mu m$ was determined the optimal one to reach the target thickness with the minimum possible printed layers. The effect of the substrate temperature on the final profilometry, walls verticality and final thickness was explored and results have shown that increasing the chuck temperature favored a better material redistribution along the printed profile, improvement of walls verticality and less material broadening, due to a faster solvent evaporation. Ultimately, a further improvement of walls verticality was achieved adopting a step-reticulation approach, which sensibly improved the final printing resolution. Given these results, prints were performed on the patterned wafer featuring the MEMS devices. Floating springs with different printed material thickness were tested in terms of their mechanical deflection and results have shown that the material quantity printed on top didn't affect their mechanical properties, thus not altering the structure stress and providing vibration damping. Further explorations of the work will consist in adopting an industrial printhead with hundreds of nozzles, in order to produce hundreds of devices within a smaller amount of time. This will sensibly contribute to the industrialization of the approach.

Table 2
Deflection of the spring according to the number of printed layers.

Die ID	Number of layers	Deflection value (μm)	Minimum value (μm)	Maximum value (μm)
128,119	1	−4.63	−4.70	−4.56
129,119	2	−5.21	−5.23	−5.17
130,119	3	−6.50	−7.42	−5.35
131,119	4	−8.61	−9.71	−7.43
132,119	5	−12.55	−13.09	−11.34

CRediT authorship contribution statement

Prisca Viviani: Conceptualization, Data curation, Investigation, Methodology, Writing – original draft, Writing – review & editing. **Maria Teresa Caporaso:** Investigation. **Martina Scolari:** Investigation, Methodology. **Ilaria Gelmi:** Investigation, Methodology. **Laura Castoldi:** Investigation, Methodology. **Luca Magagnin:** Conceptualization, Methodology, Resources, Supervision, Validation, Writing – original draft, Writing – review & editing.

Declaration of competing interest

The authors declare that they have no known competing financial interests or personal relationships that could have appeared to influence the work reported in this paper.

Appendix A. Supplementary data

Supplementary data to this article can be found online at https://doi.org/10.1016/j.jmapro.2024.04.079.

References

[1] Bhushan B, Caspers M. Microsyst Technol 2017;23:1117.
[2] Sele CW, von Werne T, Friend RH, Sirringhaus H. Adv Mater 2005;17:997.
[3] Lau G-K, Shrestha M. Micromachines 2017;8:194.
[4] Martin GD, Hoath SD, Hutchings IM. J Phys: Conf Ser 2008;105:012001.
[5] Scoutaris N, Ross S, Douroumis D. Pharm Res 2016;33:1799.
[6] Zhu X, Ng LWT, Hu G, Wu T-C, Um D-S, Macadam N, et al. Adv Funct Mater 2020;30:2002339.
[7] Mikkonen R, Puistola P, Jönkkäri I, Mäntysalo M. ACS Appl Mater Interfaces 2020;12:11990.
[8] Li G, Meng Z, Qian J, Ho C-L, Lau SP, Wong W-Y, et al. Mater Today Energy 2019;12:155.
[9] Huang T-T, Wu W. J Mater Chem A 2019;7:23280.
[10] Wen D, Wang X, Liu L, Hu C, Sun C, Wu Y, et al. ACS Appl Mater Interfaces 2021;13:17766.
[11] Campbell PG, Weiss LE. Expert Opin Biol Ther 2007;7:1123.
[12] Calvert P. Chemistry of Materials-CHEM MATER 2001:13. https://doi.org/10.1021/cm0101632.
[13] Zhou Z, Ruiz Cantu L, Chen X, Alexander MR, Roberts CJ, Hague R, et al. Addit Manuf 2019;29:100792.
[14] Nayak L, Mohanty S, Nayak SK, Ramadoss A. J Mater Chem C 2019;7:8771.
[15] Moon SJ, Robin M, Wenlin K, Yann M, Bae BS, Mohammed-Brahim T, et al. Flex Print Electron 2017;2:035008.
[16] Tekin E, Smith PJ, Schubert US. Soft Matter 2008;4:703.
[17] de Gans B-J, Schubert US. Langmuir 2004;20:7789.
[18] Liu Y, Cui T, Varahramyan K. Solid-State Electron 2003;47:1543.
[19] Chen W-C, Wu T-J, Wu W-J, Su G-DJ. J Micromech Microeng 2013;23:065008.
[20] Robin M, Kuai W, Amela-Cortes M, Cordier S, Molard Y, Mohammed-Brahim T, et al. ACS Appl Mater Interfaces 2015;7:21975.
[21] Liu Q, Le MQ, Richard C, Liang R, Cottinet P-J, Capsal J-F. Org Electron 2019;67:259.
[22] Du Z, Yu X, Han Y. Chin Chem Lett 2018;29:399.
[23] Bernasconi R, Angeli MC, Mantica F, Carniani D, Magagnin L. Polymer 2019;185:121933.
[24] Trindade MA, Benjeddou A. J Vib Control 2002;8:699.
[25] Choudhary N, Kaur D. J Nanosci Nanotechnol 1907;2015:15.
[26] Singh R, Ghosh A, Kant R, Asfar M, Bhattacharya B, Panigrahi P, et al. J Microelectromech Syst 2013;22:695.

[27] Ning H, Deng P, Yang C, Yao R, Tao R, Chen J, et al. Mol Cryst Liq Cryst 2018;676:36.
[28] Jang D, Kim D, Moon J. Langmuir 2009;25:2629.
[29] Reis N, Ainsley C, Derby B. J Appl Phys 2005;97:094903.
[30] Yunker PJ, Still T, Lohr MA, Yodh AG. Nature 2011;476:308.
[31] Soltman D, Subramanian V. Langmuir 2008;24:2224.
[32] Shimoni A, Azoubel S, Magdassi S. Nanoscale 2014;6:11084.
[33] Mampallil D, Eral HB. Adv Colloid Interface Sci 2018;252:38.
[34] Zhang Z, Zhang X, Xin Z, Deng M, Wen Y, Song Y. Adv Mater 2013;25:6714.
[35] Al-Milaji KN, Zhao H. J Phys Chem C 2019;123:12029.
[36] Sun J, Bao B, He M, Zhou H, Song Y. ACS Appl Mater Interfaces 2015;7:28086.